

Quantum 120° model on pyrochlore lattice: orbital ordering in MnV_2O_4

Gia-Wei Chern,¹ Natalia Perkins,¹ and Zhihao Hao²

¹*Department of Physics, University of Wisconsin, Madison, Wisconsin 53706, USA*

²*Department of Physics and Astronomy, Johns Hopkins University, Baltimore, Maryland 21218, USA*

(Dated: January 3, 2010)

We present an analytical model of orbital ordering in vanadium spinel MnV_2O_4 . The model is based on recent first-principles calculation indicating a strong trigonal distortion at the vanadium sites of this compound [Phys. Rev. Lett. **102**, 216405 (2009)]. At the single-ion level, the trigonal crystal field leaves a doubly degenerate atomic ground state and breaks the approximate rotational symmetry of t_{2g} orbitals. We find that the effective interaction between the low-energy doublets is described by a quantum antiferromagnetic 120° model on the pyrochlore lattice. We obtain the classical ground state and show its stability against quantum fluctuations. The corresponding orbital order consisting of two inequivalent orbital chains is consistent with the experimentally observed tetragonal symmetry. A periodic modulation of electron density function along orbital chains is shown to arise from the staggering of local trigonal axes. In the presence of orbital order, single-ion spin anisotropy arising from relativistic spin-orbit interaction stabilizes the experimentally observed orthogonal magnetic structure.

I. INTRODUCTION

Geometrically frustrated magnets with orbital degeneracy exhibit a variety of complex ground states with unusual magnetic and orbital orders.^{1–4} Not only do these spin-orbital models deepen our understanding of systems with competing degrees of freedom, they also describe the low-energy physics of several transition-metal compounds. Of particular interest is spin-orbital model on three-dimensional pyrochlore lattice,^{5,6} where geometrical frustration between nearest-neighbor spins leads to a macroscopic degeneracy in the classical ground state.⁷ Experimentally, a signature of strong frustration is the occurrence of a magnetic phase transition well below the Curie-Weiss temperature. For systems with degenerate orbitals, magnetic frustration is partially relieved in the presence of a long-range orbital order, which is usually accompanied by a simultaneous structural distortion due to Jahn-Teller effect. The resulting magnetic order depends critically on the orbital configuration and the details of spin-orbital interactions.

Recently, much attention has been focused on vanadium spinels AV_2O_4 , where vanadium ions occupying the structural B -sites form a pyrochlore lattice.^{8–15} The two d electrons of V^{3+} ion have a total spin $S = 1$ and occupy two out of three t_{2g} orbitals. Thermodynamically, vanadium spinels with a non-magnetic A -site ion ($A = \text{Zn}, \text{Cd}, \text{and Mg}$) exhibit similar behavior: a structural transition which lowers the crystal symmetry from cubic $Fd\bar{3}m$ to tetragonal $I4_1/amd$ is followed by a magnetic ordering at a lower temperature.^{8–10} Assuming that xy orbital is occupied at all sites due to flattened VO_6 octahedra, minimization of a Kugel-Khomskii type Hamiltonian on pyrochlore lattice gives rise to a staggered ordering of the remaining yz and zx orbitals (so-called A -type ordering).¹⁶ The resulting symmetry $I4_1/a$, however, is incompatible with experimental observations.

On the other hand, assuming a large relativistic spin-orbit coupling, a ferro-orbital order in which one electron

occupies the low-energy xy orbital, whereas the other one is in states $|yz\rangle \pm i|zx\rangle$ has been proposed in Ref. 17. The occurrence of complex orbitals imply a nonzero orbital angular momentum. This model successfully explains important experimental results: the uniform occupation of orbitals is compatible with space group $I4_1/amd$; an ordering of orbital moment opposite to local spin direction is also consistent with the observed reduced vanadium moment. A ground state with complex orbitals has also been confirmed by mean-field¹⁸ and *ab initio* calculations.^{19,20}

Interest in antiferro-orbital order is rekindled by a recent experimental characterization of another vanadium spinel MnV_2O_4 ,^{12–15} where the A -site Mn^{2+} ion is in a $3d^5$ high spin configuration ($S = 5/2$). In contrast to other vanadium spinels, MnV_2O_4 first undergoes a magnetic transition at $T_F = 56$ K into a collinear ferrimagnetic phase with Mn and V moments aligned antiparallel to each other. At a slightly lower temperature $T_S = 53$ K, a structural distortion lowering the crystal symmetry to tetragonal $I4_1/a$ is accompanied by an ordering of the transverse components of V spins. The ground-state orbital configuration is suggested to be the A -type antiferro-orbital order.¹⁴ Also contrary to collinear magnetic order in other vanadium spinels, a peculiar non-collinear order with transverse component of vanadium spins forming an orthogonal structure in the ab plane was observed in MnV_2O_4 .^{14,15}

Recently we have demonstrated the stability of orthogonal magnetic structure in the limit of strong relativistic spin-orbit coupling.^{21,22} However, findings from first-principles calculation indicate a significant trigonal distortion at the vanadium sites of MnV_2O_4 ,²³ whose effect is yet to be understood. The same authors find an orbital order consisting of two inequivalent orbital chains similar to the A -type order. More importantly, they observe an additional modulation of electron density profile *within* each orbital chain: the orbitals rotate alternatively by about 45° along the chain. This complex orbital pattern

is also supported by a recent NMR measurement.²⁴

Based on these observations, we present an analytical model of spinel MnV_2O_4 assuming that the t_{2g} orbitals is split into a singlet and a doublet by a strong trigonal crystal field. As one electron occupies the low-energy a_{1g} orbital, a double degeneracy remains for the other electron. After introducing a pseudospin-1/2 to describe the doubly degenerate atomic ground state, we find that their effective interaction is governed by a highly anisotropic quantum 120° Hamiltonian.^{25,26} By treating quantum fluctuations using the semiclassical framework, the classical ground state of the 120° model is shown to be stable against quantum fluctuations. Orbital ordering and lattice distortion derived from the classical ground states are consistent with the experiments. We also shown that an alternatively rotated orbital basis due to the staggered trigonal axes explains the periodic density-modulation observed in *ab initio* calculations. Moreover, since the very presence of trigonal distortion breaks the (approximate) rotational symmetry of t_{2g} orbitals, orthogonal magnetic structure thus comes naturally from spin-orbit interaction and the staggering of trigonal axes.

The rest of the paper is organized as follows. Sec. II discusses the effective orbital 120° model on pyrochlore lattice and its semiclassical ground states. The corresponding orbital order and lattice distortion are discussed in Sec. III. The modulation of electron density function along orbital chain is addressed in Sec. IV. The details of magnetic structure is presented in Sec. V. And finally Sec. VI presents a conclusion.

II. 120° MODEL

The site symmetry of vanadium ions in most vanadates is dominated by a cubic crystal field. Nonetheless, splitting of t_{2g} triplet due to an additional trigonal distortion is known to play an important role in some cases. Most notably, stabilization of the unusual magnetic structure in the insulating phase of V_2O_3 can only be understood when the trigonal splitting is properly taken into account.²⁷⁻²⁹ The effects of trigonal distortions in vanadium spinels vary from one compound to another. For example, the trigonal splitting of t_{2g} levels is essential to the understanding of heavy fermion behavior in metallic LiV_2O_4 .³⁰ On the other hand, it seems to have a negligible effect in another well-studied spinel ZnV_2O_4 .¹⁹

Recently, experiment¹⁵ and *ab initio* calculation²³ both indicate a strong trigonal distortion at the vanadium sites of MnV_2O_4 . In order to understand its effects at least qualitatively and to make analytical calculations tractable, we consider the limit of a dominating trigonal crystal field in this paper. As discussed in the introduction, the trigonal distortion still leaves a doubly degenerate atomic ground state. The possible long-range order of these localized doublets is investigated using the effective Hamiltonian approach. By studying the ground

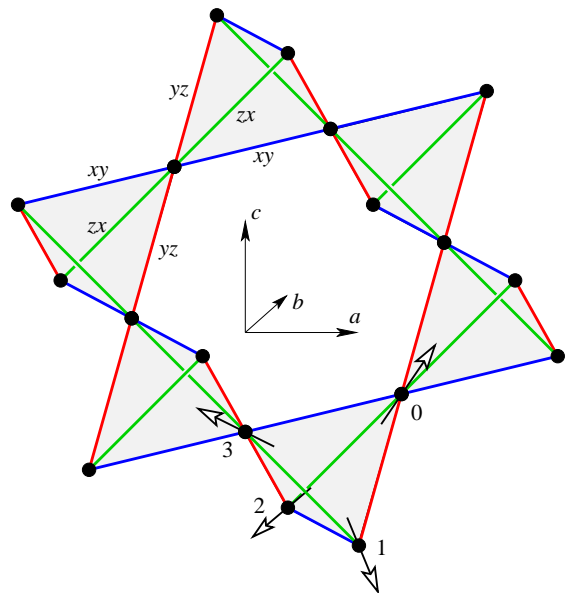


FIG. 1: Pyrochlore lattice. The numbers 0-3 denotes the four sublattices of pyrochlore lattice; the arrows indicate the local C_3 axis of the respective sublattices. Explicitly, they are $\hat{\nu}_0 = [111]$, $\hat{\nu}_1 = [\bar{1}\bar{1}\bar{1}]$, $\hat{\nu}_2 = [\bar{1}1\bar{1}]$, and $\hat{\nu}_3 = [\bar{1}\bar{1}1]$. In 120° -model Eq. (6), orbital interactions on red, green, and blue bonds are characterized by vectors \hat{n}_{yz} , \hat{n}_{zx} , and \hat{n}_{xy} , respectively.

state of the effective model, we discuss its implications for orbital and magnetic ordering in MnV_2O_4 .

In the presence of a trigonal distortion, the crystal field of reduced site symmetry (from cubic O_h to D_{3d}) splits t_{2g} orbitals into a singlet and a doublet separated by an energy gap Δ . The C_3 symmetry axis of D_{3d} group is parallel to the local $\langle 111 \rangle$ direction of the ion (Fig. 1). The a_{1g} singlet is the symmetric linear combination of t_{2g} orbitals under C_3 rotation

$$|a_{1g}\rangle = \nu_x|yz\rangle + \nu_y|zx\rangle + \nu_z|xy\rangle, \quad (1)$$

where $\hat{\nu} = (\nu_x, \nu_y, \nu_z)$ is a unit vector parallel to the local trigonal axis (Fig. 1). We use the following chiral basis for the e_g doublet

$$\begin{aligned} |e_g^+\rangle &= \nu_x e^{-i\omega}|yz\rangle + \nu_y e^{+i\omega}|zx\rangle + \nu_z|xy\rangle, \\ |e_g^-\rangle &= \nu_x e^{+i\omega}|yz\rangle + \nu_y e^{-i\omega}|zx\rangle + \nu_z|xy\rangle, \end{aligned} \quad (2)$$

where $\omega = 2\pi/3$. A complete basis for V^{3+} ion with $3d^2$ configuration is given by $|a_{1g}e_g^+\rangle$, $|a_{1g}e_g^-\rangle$, and $|e_g^+e_g^-\rangle$. Here the two-electron state is defined as the antisymmetric sum of individual one-electron states, i.e. $|\alpha\beta\rangle \equiv (|\alpha\rangle|\beta\rangle - |\beta\rangle|\alpha\rangle)/\sqrt{2}$. Since the a_{1g} singlet has the lowest energy, the atomic ground state is doubly degenerate. To describe the low-energy doublet manifold, we introduce a pseudospin- $\frac{1}{2}$ operator τ such that $|\tau_z = \pm 1\rangle$ are identified with $|a_{1g}e_g^\pm\rangle$, respectively.

In vanadium spinels, the superexchange (SE) interaction with a 90° angle between vanadium-oxygen bonds

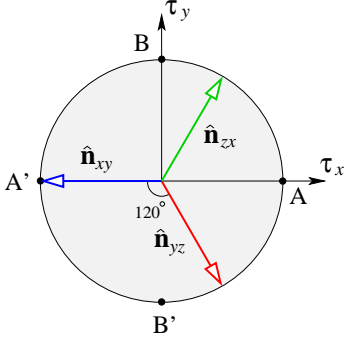


FIG. 2: Unit circle in the (τ_x, τ_y) plane. Pseudospins τ_i participate in the 120° interaction (6) only through their projections onto the three unit vectors $\hat{\mathbf{n}}_{yz}$, $\hat{\mathbf{n}}_{zx}$, and $\hat{\mathbf{n}}_{xy}$.

is dominated by direct exchange which involves electron hopping of the $dd\sigma$ type:^{16,18}

$$H_{SE} = - \sum_{\langle ij \rangle} \left\{ J_2 (1 - \mathbf{S}_i \cdot \mathbf{S}_j) P_{\alpha,i} P_{\alpha,j} + (J_0 \mathbf{S}_i \cdot \mathbf{S}_j + J_1) [P_{\alpha,i} (1 - P_{\alpha,j}) + (1 - P_{\alpha,i}) P_{\alpha,j}] \right\}. \quad (3)$$

The various exchange constants are $J_0 = J\eta/(1 - 3\eta)$, $J_1 = J(1 - \eta)/(1 - 3\eta)$, and $J_2 = J(1 + \eta)/(1 + 2\eta)$, where $J = t_{dd\sigma}^2/U$ sets the overall energy scale and $\eta = J_H/U \approx 0.11$ denotes the ratio of Hund's exchange to on-site Coulomb repulsion. The subscript $\alpha \equiv \alpha(ij)$ of the projection operators specifies the type of orbitals in which electron hopping is possible between sites i and j , e.g. $\alpha(ij) = xy$ for nearest-neighbor bonds on $\langle 110 \rangle$ and $\langle \bar{1}\bar{1}0 \rangle$ chains (blue bonds in Fig. 1).

An interesting feature of Hamiltonian (3) is the static Potts-like orbital interactions which depend only on orbital projection operators P_{xy} , P_{yz} , and P_{zx} . Restricted to the doublet manifold $|\tau_z = \pm 1\rangle$, they become

$$P_\alpha = \frac{2}{3} - \frac{1}{3} \boldsymbol{\tau} \cdot \hat{\mathbf{n}}_\alpha, \quad (4)$$

where the three unit vectors are (Fig. 2):

$$\hat{\mathbf{n}}_{yz} = \frac{1}{2} \hat{\mathbf{x}} - \frac{\sqrt{3}}{2} \hat{\mathbf{y}}, \quad \hat{\mathbf{n}}_{zx} = \frac{1}{2} \hat{\mathbf{x}} + \frac{\sqrt{3}}{2} \hat{\mathbf{y}}, \quad \hat{\mathbf{n}}_{xy} = -\hat{\mathbf{x}}. \quad (5)$$

A remark is now in order: the restricted Hilbert space $|\pm\rangle$ already precludes descriptions of, e.g. the A -type antiferro-orbital order consisting of alternating $|xy, yz\rangle$ and $|xy, zx\rangle$ states.¹⁶ A more general approach is to introduce a pseudospin-1 formulation similar to the one used in Ref. 29; the trigonal splitting is then modeled by a spin anisotropy term. However, the resulting effective Hamiltonian is quite complicated and analytical calculations are difficult. In this paper, we choose the simplified pseudospin- $\frac{1}{2}$ formulation to explore the essential features of a large trigonal distortion and use perturbation method to examine the effect of excited state $|e_g^+ e_g^-\rangle$.

The effective Hamiltonian H_{eff} of pseudospins $\boldsymbol{\tau}$ can be obtained by projecting SE Hamiltonian onto the doublet

manifold, or equivalently by substituting the projection operators (4) into Eq. (3). In order to understand the intrinsic properties of orbital interaction, we first examine H_{eff} above the structural transition T_S , where nearest-neighbor spin correlations $\langle \mathbf{S}_i \cdot \mathbf{S}_j \rangle$ are isotropic. For example, below the Curie-Weiss temperature, the magnet is in a strongly correlated liquid-like state,⁷ the constraint of zero total spin $\mathbf{S}_{\boxtimes} = 0$ on every tetrahedron gives a spin correlation $\langle \mathbf{S}_i \cdot \mathbf{S}_j \rangle = -S^2/3$. In the collinear ferrimagnetic phase, a partial ferromagnetic order \mathbf{M} antiparallel to the Mn moments is induced by the antiferromagnetic Mn-V exchange; the spin correlation becomes $\langle \mathbf{S}_i \cdot \mathbf{S}_j \rangle = -S^2/3 + M^2$. In all cases, the effective orbital interaction has the following anisotropic form:

$$H_{\text{eff}} = J_\tau \sum_{\langle ij \rangle} (\boldsymbol{\tau}_i \cdot \hat{\mathbf{n}}_\alpha) (\boldsymbol{\tau}_j \cdot \hat{\mathbf{n}}_\alpha), \quad (6)$$

where $J_\tau = \frac{1}{9} [2J_1 - J_2 + \langle \mathbf{S}_i \cdot \mathbf{S}_j \rangle (J_2 + 2J_0)] > 0$ and $\alpha = \alpha(ij) = yz, zx$, and xy depending on the orientation of the nearest-neighbor bond (Fig. 1). The effective Hamiltonian has a form of the so-called 120° model,^{25,26} which was first introduced as an effective model for perovskite e_g orbital systems.³¹⁻³³ Recently, the same model was found to describe the insulating phase of p -band fermions in optical lattices.^{34,35} The 120° model is closely related to the well-known quantum compass model.³⁶ A common feature shared by these highly anisotropic spin models is the competition between bonds along different directions. For compass and 120° models on bipartite lattices, a macroscopic degeneracy of the ground state results from the discrete gauge-like sliding symmetries.³⁷ Remarkably, as discussed in more detail below, such extensive degeneracy is absent in the classical 120° model on non-bipartite pyrochlore lattice.

We first discuss the origin of the macroscopic degeneracy in the cubic lattice 120° model. The three unit vectors $\hat{\mathbf{n}}_\alpha$ in Eq. (5) are associated with nearest-neighbor bonds along x , y , and z directions, respectively.³² The bipartite nature of the cubic lattice allows us to transform an antiferromagnetic coupling to a ferromagnetic one through a π -rotation about τ_z axis on one sublattice. An unusual property of the classical model is the appearance of planar gauge-like symmetries in addition to global spin rotations.^{25,26} A huge ground-state degeneracy thus results from the gauge-like Z_2 transformations. As demonstrated in Ref. 26, starting from a state of uniform spins, which is a ground state of the ferromagnetic model, another inequivalent ground state can be obtained by rotating all spins on a randomly chosen xy plane by an angle π about τ_x axis. Nonetheless, long-range order arises via the order-by-disorder mechanism which in general favors collinear (uniform) spin configurations.²⁵

Interestingly, the above-mentioned gauge-like symmetry is absent for 120° model on pyrochlore lattice. This is because a prerequisite for the Z_2 gauge-like transformation is the existence of a subset \mathcal{C} of lattice sites (e.g., planes or chains) such that pseudospins belonging to the subset are connected to each other by, say, either yz or

zx bonds, while interaction of pseudospin $i \in \mathcal{C}$ with its neighbor $j \notin \mathcal{C}$ is of the xy type exclusively. It could be easily checked that such a subset cannot be found in pyrochlore lattice. However, orbital interactions are still frustrated simply due to geometry: antiferromagnetic pseudospin interaction cannot be satisfied on all nearest-neighbor bonds simultaneously.³⁸

Despite being geometrically frustrated, the strong anisotropy of 120° interaction significantly reduces the number of degenerate ground states. To see this, we note that the energy of a single bond is minimized classically by a pair of pseudospins pointing toward $\pm \hat{\mathbf{n}}_\alpha$, respectively, where $\hat{\mathbf{n}}_\alpha$ is the unit vector characterizing the anisotropic interaction of the bond. However, such absolute minimum can not be attained at every nearest-neighbor bonds due to geometrical frustration. Even worse, pseudospin correlation on some bonds is frustrated, i.e. $\tau_i \cdot \tau_j > 0$. In order to minimize the energy cost, frustrated pseudospins thus tend to align themselves perpendicular to $\hat{\mathbf{n}}_\alpha$. Through both analytical calculation and Monte-Carlo simulations, we find that collinear states with pseudospins perpendicular to either one of the three $\hat{\mathbf{n}}_\alpha$ are the classical ground states (Fig. 3). The total degeneracy is six due to an additional C_2 -rotation about τ_z axis. This is in stark contrast to the macroscopic ground-state degeneracy of classical Heisenberg spins on the pyrochlore lattice.⁷

The three inequivalent ground states shown in Fig. 3 are characterized by the locations of frustrated bonds. More specifically, we introduce three staggered order parameters³⁹

$$\begin{aligned} \mathbf{l}_{yz} &= (\tau_0 + \tau_1 - \tau_2 - \tau_3)/4, \\ \mathbf{l}_{zx} &= (\tau_0 - \tau_1 + \tau_2 - \tau_3)/4, \\ \mathbf{l}_{xy} &= (\tau_0 - \tau_1 - \tau_2 + \tau_3)/4 \end{aligned} \quad (7)$$

to describe the orbital order. Here τ_i denotes pseudospin average on i th sublattice. These order parameters measure the difference of orbital configuration on bonds of the same type. For example, a nonzero \mathbf{l}_{xy} indicates an antiferro-orbital order across the two xy bonds of a tetrahedron [see Fig. 3(c)]. The nonzero order parameter characterizing the collinear states of Fig. 3 are: (a) $\mathbf{l}_{yz} = -\frac{\sqrt{3}}{2}\hat{\mathbf{x}} - \frac{1}{2}\hat{\mathbf{y}}$, (b) $\mathbf{l}_{zx} = -\frac{\sqrt{3}}{2}\hat{\mathbf{x}} + \frac{1}{2}\hat{\mathbf{y}}$, and (c) $\mathbf{l}_{xy} = \hat{\mathbf{y}}$. This should be contrasted with the continuously degenerate collinear ground states in Heisenberg model, i.e. $\mathbf{l}_\alpha = \hat{\mathbf{e}}$ with $\hat{\mathbf{e}}$ being an arbitrary unit vector.³⁹

The stability of classical ground states in the presence of quantum fluctuations is investigated using the semiclassical Holstein-Primakoff transformation. We find that the anisotropy of the orbital exchange leads to a gapped quasiparticle spectrum in the whole Brillouin zone. At the harmonic level, quantum fluctuations around collinear ground states are shown to give a negligible correction to the sublattice ‘magnetization’ $\langle \tau_i \rangle$ (about 4%), indicating the stability of the classical ground states. A detailed account of the semiclassical calculation is presented in Appendix B.

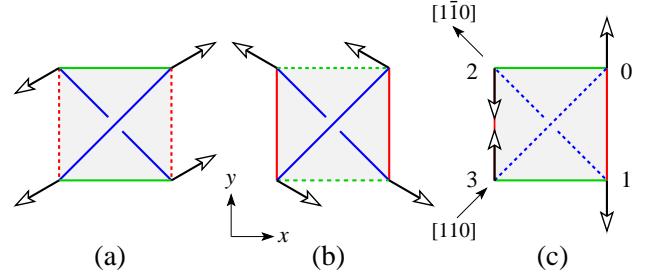


FIG. 3: Ground states of the orbital 120° -model. The other three ground states are related to the above ones by a C_2 rotation of pseudospins about the z axis. Orbital interactions on red, green, and blue bonds are characterized by vector \mathbf{n}_{yz} , \mathbf{n}_{zx} , and \mathbf{n}_{xy} , respectively. The frustrated bonds (parallel pseudospins) are indicated by dashed lines. Nonzero order parameter characterizing the ground states are: (a) $\mathbf{l}_{yz} = -\frac{\sqrt{3}}{2}\hat{\mathbf{x}} - \frac{1}{2}\hat{\mathbf{y}}$, (b) $\mathbf{l}_{zx} = -\frac{\sqrt{3}}{2}\hat{\mathbf{x}} + \frac{1}{2}\hat{\mathbf{y}}$, and (c) $\mathbf{l}_{xy} = \hat{\mathbf{y}}$.

Before closing this section, we remark that phonon-mediated orbital exchange in spinels also has the form of 120° interaction with an effective exchange $J_\tau \propto g^2/k_{F_{1g}}$, where g is a Jahn-Teller coupling constant and $k_{F_{1g}}$ is the elastic constant of F_{1g} phonons.²¹ Detailed derivation is presented in Appendix A. In fact, noting that (τ_x, τ_y) forms a doublet irreducible representation of D_{3d} group, the 120° type interaction in Eq. (6) is the only anisotropic pseudospin interaction allowed by lattice symmetry. In this perspective, we shall regard J_τ as an effective model parameter in the following discussion.

III. ORBITAL ORDER AND LATTICE DISTORTION

We now discuss the orbital order and lattice distortions corresponding to the semiclassical ground states. Specifically, we shall focus on the collinear state characterized by $\mathbf{l}_{xy} = +\hat{\mathbf{y}}$ [Fig. 3(c)]. Since $P_{yz} + P_{zx} + P_{xy} = 2$, orbital orders are essentially described by linear combinations

$$\begin{aligned} P_1 &= P_{yz} + P_{zx} - 2P_{xy} = -\tau_x, \\ P_2 &= \sqrt{3}(P_{zx} - P_{yz}) = -\tau_y, \end{aligned} \quad (8)$$

which transform as a doublet irreducible representation under symmetry group D_{3d} . Since pseudospins pointing along $\pm y$ directions are sitting on $[110]$ and $[\bar{1}\bar{1}0]$ chains, respectively, the ground state shown in Fig. 3(c) consists of two distinct orbital chains characterized by $P_1 = 0$, $P_2 = \mp 1$, respectively. The staggered part P_2 of the orbital order comes from the occupation difference between yz and zx orbitals. The uniform part given by $P_{yz} = P_{zx} = P_{xy} = 2/3$ indicates that the three orbitals are equally occupied on average.

Due to Jahn-Teller effect, a long-range orbital order also implies a lattice distortion in the ground state, which is indeed observed in MnV_2O_4 below $T_S = 53$ K. On symmetry ground, the coupling between orbital doublet

$|\tau_z = \pm 1\rangle$ and distortions of the surrounding VO_6 octahedron has the form:

$$V_{\text{JT}} = -g(\delta_1 \tau_x + \delta_2 \tau_y), \quad (9)$$

where (δ_1, δ_2) are coordinates of normal modes transforming as an e_g representation of group D_{3d} . The two symmetry-breaking modes can be thought of as analogous to the tetragonal and orthorhombic distortions in a cubic VO_6 octahedron. The energy cost associated with the distortion is $\frac{k}{2}(\delta_1^2 + \delta_2^2)$, where k is an effective elastic constant. For orbital order characterized by $\mathbf{l}_{xy} = +\hat{\mathbf{y}}$, minimization with respect to phonons yields distortions described by $\delta_1 = 0$ and $\delta_2 = \pm g/k$ on the two inequivalent orbital chains: octahedra on $[110]$ and $[1\bar{1}0]$ chains are elongated along the x and y axes, respectively. The overall distortion preserves the tetragonal symmetry (lattice constants $a = b > c$) and is consistent with the observed space group $I4_1/a$.¹⁴

It is interesting to note that the staggered orthorhombic distortions of VO_6 octahedra actually correspond to a softened $\mathbf{q} = 0$ lattice phonons with F_{1g} symmetry.^{21,40} This is consistent with the fact that, by integrating out F_{1g} phonons, orbital Jahn-Teller coupling gives the same 120° pseudospin interaction (Appendix A). In this respect, orbital ordering and structural transition in MnV_2O_4 can also be viewed as softening of F_{1g} phonons due to cooperative Jahn-Teller effect.

Despite the similarities between the antiferro-orbital order of 120° model and the A -type order proposed in Ref. 16, inclusion of spin-orbit interaction illustrates an important difference between the two cases. As we shall discuss later, spin-orbit coupling gives rise to an orthogonal magnetic order in 120° model, which is in stark contrast to collinear spins in the case of A -type orbital order.

IV. MODULATION OF ELECTRON DENSITY FUNCTION

The staggering of trigonal axes along orbital chains also results in a periodic variation of electron density distributions, despite the orbital occupation numbers are invariant within the chain. This is because the actual orbital wavefunction corresponding to $\boldsymbol{\tau} = \pm\hat{\mathbf{y}}$ also depends on the local C_3 axis:

$$\begin{aligned} |\tau_y = +1\rangle &= \sqrt{2}(\nu_x \cos \xi |X\rangle + \nu_y \sin \xi |Y\rangle) + \nu_z |Z\rangle, \\ |\tau_y = -1\rangle &= \sqrt{2}(\nu_x \sin \xi |X\rangle + \nu_y \cos \xi |Y\rangle) + \nu_z |Z\rangle. \end{aligned} \quad (10)$$

Here the angle ξ is defined by $\tan \xi = (1 - \sqrt{3})/(1 + \sqrt{3})$, and $|X\rangle = |zx, xy\rangle$, $|Y\rangle = |xy, yz\rangle$ and $|Z\rangle = |yz, zx\rangle$ are the two-electron basis introduced in Ref. 17. Note that since τ_z is diagonal in the chiral basis $|\pm\rangle$, eigenstates of τ_y are composed of real orbitals.

We now consider orbital chains running along $[110]$ direction, in which the local C_3 axis alternates between $\hat{\nu}_0$ and $\hat{\nu}_3$ [Fig. 3(c)]. Along the chain, the electrons are in

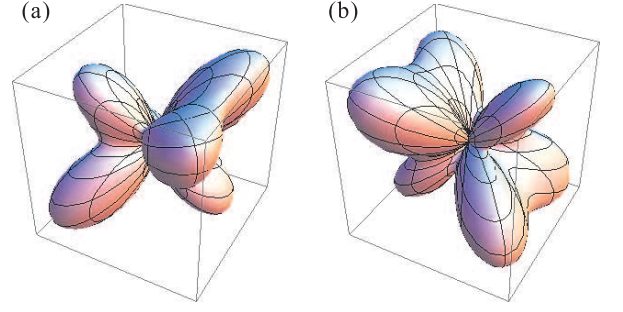


FIG. 4: Electron density of state $|\tau_y = +1\rangle$ with trigonal axis along (a) $\hat{\nu}_0 = [111]$ and (b) $\hat{\nu}_3 = [\bar{1}\bar{1}\bar{1}]$ directions. The explicit forms of the density corresponding to (a) and (b) are $\rho_0(\mathbf{r}) \pm \delta\rho(\mathbf{r})$, respectively.

the $|\tau_y = +1\rangle$ state whose electron density can be readily computed

$$\begin{aligned} \rho(\mathbf{r}) &= \frac{1}{2} \sum_{i=1,2} \int \delta(\mathbf{r} - \mathbf{r}_i) |\langle \mathbf{r}_1, \mathbf{r}_2 | \tau_y = +1 \rangle|^2 d^3 r_1 d^3 r_2 \\ &= \rho_0(\mathbf{r}) \pm \delta\rho(\mathbf{r}), \end{aligned} \quad (11)$$

where the $+$ and $-$ signs refer to sites with $\hat{\nu}_0$ and $\hat{\nu}_3$ trigonal axes, respectively. Introducing basis functions, e.g. $\psi_{xy}(\mathbf{r}) = f(r)xy$, where $f(r)$ is a spherically symmetric function, the uniform and staggered parts of electron density are given by

$$\begin{aligned} \rho_0(\mathbf{r}) &= \frac{1}{3} \psi_{xy}^2(\mathbf{r}) - \frac{2}{3} \cos \xi \sin \xi \psi_{yz}(\mathbf{r}) \psi_{zx}(\mathbf{r}) \\ &\quad + \left(\frac{1}{2} - \frac{1}{3} \cos^2 \xi \right) \psi_{yz}^2(\mathbf{r}) + \left(\frac{1}{2} - \frac{1}{3} \sin^2 \xi \right) \psi_{zx}^2(\mathbf{r}), \end{aligned} \quad (12)$$

$$\delta\rho(\mathbf{r}) = \frac{-1}{3\sqrt{2}} \psi_{xy}(\mathbf{r}) \left(\sin \xi \psi_{yz}(\mathbf{r}) + \cos \xi \psi_{zx}(\mathbf{r}) \right). \quad (13)$$

The resulting density functions are plotted in Fig. 4. A similar density modulation, in which orbitals rotate alternatively by about 45° along the orbital chain, is also observed in first-principle density functional calculations.²³

The periodic modulation of the electron density functions along orbital chains is a natural consequence of the staggering of local symmetry axes. In contrast, such density-modulation is absent in other orbital orders proposed for vanadium spinels. In A -type order, the two orbital chains are characterized by occupied two-electron states $|X\rangle$ and $|Y\rangle$, respectively. Along a given chain, e.g. the $|X\rangle$ chain, the electron density $\rho(\mathbf{r}) = \frac{1}{2} \psi_{zx}^2(\mathbf{r}) + \frac{1}{2} \psi_{xy}^2(\mathbf{r})$ is invariant. In the ferro-orbital order proposed as the ground state of ZnV_2O_4 ,¹⁷ there is only one type of orbital chain, along which the two electrons occupy states $\frac{1}{\sqrt{2}}(|X\rangle \pm i|Y\rangle)$ alternatively, giving rise to a staggered orbital angular momentum $\mathbf{L} = \pm\hat{\mathbf{z}}$. Despite the π -phase modulation, the electron density $\rho(\mathbf{r}) = \frac{1}{2} \psi_{xy}^2(\mathbf{r}) + \frac{1}{4} (\psi_{yz}^2(\mathbf{r}) + \psi_{zx}^2(\mathbf{r}))$ is the same at all sites.

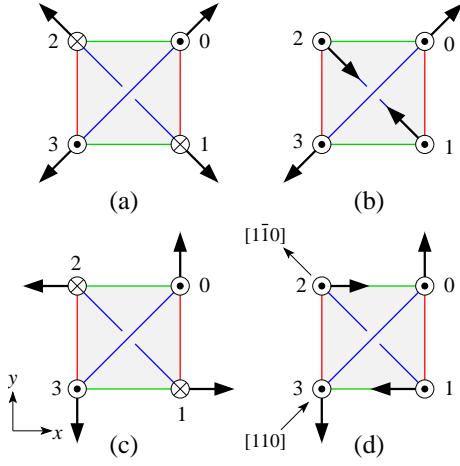


FIG. 5: Magnetic orders of vanadium spinels. The \odot and \otimes symbols denote $\pm S_z$ components, respectively. In the limit $\Delta \gg \lambda \gg J_\tau$, the spin anisotropy is dominated by Eq. (15), and the in-plane spins point along diagonal directions $S_x = \pm S_y$. The corresponding magnetic orders are shown in (a) and (b) for the case of non-magnetic and magnetic A-site ions, respectively. In the opposite limit $J_\tau \gg \Delta \gg \lambda$, spin anisotropy is governed by Eq. (17), the resulting magnetic orders are shown in (c) and (d) for the respective case of non-magnetic and magnetic A-site ions.

V. MAGNETIC ORDER

In the absence of orbital order, interaction between vanadium spins is governed by an isotropic Heisenberg model, which is known to exhibit strong geometrical frustration on pyrochlore lattice.⁷ The energy minimum of the model is attained by a macroscopically large number of states in which the total spin of every tetrahedron is zero $\mathbf{S}_\Box = 0$. The magnetic frustration is partially relieved below $T_F \approx 56$ K as the antiferromagnetic Mn-V exchange induces a ferrimagnetic order with antialigned Mn and V spins pointing along the crystal c axis. The transverse components of V spins remain disordered.

The residual frustration is relieved by anisotropic spin exchange as well as single-ion anisotropy in the presence of long-range orbital order. The anisotropic spin exchange comes from the dependence of magnetic interaction on the underlying orbital configurations, as indicated by SE Hamiltonian (3). For example, orbital order corresponding to $\mathbf{l}_{xy} = \pm \hat{\mathbf{y}}$ gives rise to an anisotropic exchange constant such that $J_{[110]} \approx \frac{4}{9}J_2$ for bonds along $[110]$ and $[1\bar{1}0]$ directions, i.e. directions of orbital chains, and $J_{[011]} = J_{[010]} \approx \frac{13}{36}J_2$ for bonds along other directions. Consequently, upon decreasing the temperature, long-range antiferromagnetic spin correlation first develops along orbital chains. However, three-dimensional magnetic order is not realized due to frustrated inter-chain couplings.

On the other hand, single-ion anisotropy resulting from the relativistic spin-orbit (SO) interaction $V_{LS} = \lambda(\mathbf{L} \cdot \mathbf{S})$ is more efficient in relieving the magnetic frustration. It

is interesting to note that the chiral basis $|e_g^\pm\rangle$ introduced in Eq. (2) are simultaneous eigenstates of angular momentum operator projected onto the local trigonal axis:

$$(\mathbf{L} \cdot \hat{\nu}) |e_g^\pm\rangle = \pm |e_g^\pm\rangle. \quad (14)$$

Restricted to the doublet subspace $|\pm\rangle$, the angular momentum operator is given by $\mathbf{L} = \hat{\nu} \tau_z$, and the effective SO interaction becomes

$$V_{LS} = \lambda(\mathbf{S} \cdot \hat{\nu}) \tau_z. \quad (15)$$

We first consider limit $\Delta \gg \lambda \gg J_\tau$, where the single-ion physics dominates the Hamiltonian. The atomic ground state is a non-Kramers doublet ($\lambda > 0$ in V^{3+} ion)

$$\begin{aligned} |\uparrow\rangle &= |\tau_z = +1\rangle \otimes |\mathbf{S} \cdot \hat{\nu} = -1\rangle, \\ |\downarrow\rangle &= |\tau_z = -1\rangle \otimes |\mathbf{S} \cdot \hat{\nu} = +1\rangle, \end{aligned} \quad (16)$$

Long-range ordering of spins and orbitals depends further on the relative strength of antiferromagnetic Mn-V and V-V exchanges.

In the case of a non-magnetic A-site ion, the ground state consists of a uniform occupation of either $|\uparrow\rangle$ or $|\downarrow\rangle$ states. It is easy to check that the resulting non-collinear spin configuration ($\mathbf{S}_i = +\hat{\nu}$ or $\mathbf{S}_i = -\hat{\nu}$) also minimizes the V-V exchange. The corresponding ferro-orbital order is characterized by order parameter $\mathbf{m}_\tau \equiv \frac{1}{4}(\tau_0 + \tau_1 + \tau_2 + \tau_3) = \mp \hat{\mathbf{z}}$. On the other hand, the Mn-V exchange is minimized by a staggering of occupied $|\uparrow\rangle$ and $|\downarrow\rangle$ states such that the S_z component at every site is opposite to Mn spins (whose effect can be thought of as an external magnetic field). The ground state can then be viewed as a collection of two inequivalent spin-orbital chains running along $[110]$ and $[1\bar{1}0]$ directions [Fig. 5(b)]. The corresponding orbital configuration is described by order parameter $\mathbf{l}_{xy} = \pm \hat{\mathbf{z}}$.

When J_τ is comparable or larger than λ , the competition between SO interaction and orbital-exchange gives rise to a $\tau_z \propto \lambda/J_\tau$. The perturbation (15) thus is essentially of order λ^2 . To be consistent, we should take into account the second-order perturbations of SO interaction simultaneously. A straightforward calculation yields

$$V'_{LS} = \frac{\lambda^2}{3\Delta} \tau_x (S_x^2 + S_y^2 - 2S_z^2) + \frac{\lambda^2}{\sqrt{3}\Delta} \tau_y (S_x^2 - S_y^2). \quad (17)$$

This expression can be thought of as an invariant product of two irreducible e_g representations of D_{3d} . Now consider ground state characterized by $\mathbf{l}_{xy} = +\hat{\mathbf{y}}$ in which pseudospins $\tau_i = \pm \hat{\mathbf{y}}$ along $[110]$ and $[1\bar{1}0]$ orbital chains, respectively. The second term in Eq. (17) thus introduces a *staggered* spin anisotropy with easy axis parallel to y or x axes depending on $\tau_y = +1$ or -1 , respectively.

To determine the equilibrium spin configuration, we note that the two competing anisotropies Eqs. (15) and (17) have a magnitude of order λ^2/J_τ and λ^2/Δ , respectively. Consequently, when orbital exchange (including phonon-mediated exchange) dominates the trigonal splitting $J_\tau \gg \Delta$, the anisotropy $\pm(S_x^2 - S_y^2)$ wins and aligns

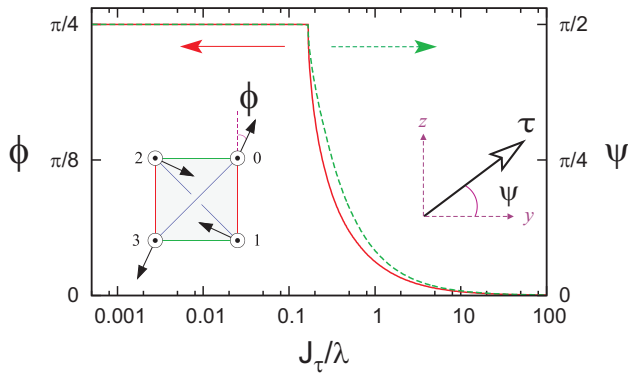


FIG. 6: Evolution of orthogonal magnetic order as a function of the ratio J_τ/λ . The parameter ψ and ϕ measure the rotation angle of pseudospin and in-plane orthogonal structure, respectively. The SO coupling constant is set to $\lambda = 0.75\Delta$, and the ferromagnetic spin component is $S_z = 1/\sqrt{3}$. The limiting cases $\phi = \pi/4$ and $\phi = 0$ correspond to magnetic orders shown in Figs. 5 (b) and (d), respectively.

spins to either x or y directions along the respective orbital chains. The resulting magnetic orders are shown in Figs. 5(c) and (d) for the case of non-magnetic and magnetic A -site ions, respectively. In particular, the one shown in Fig. 5(d) is consistent with the proposed magnetic ground state for MnV_2O_4 in Ref. 14.

In order to understand in more detail the transition between these two limiting cases, we performed an explicit calculation of the magnetic structure using Eqs. (6), (15), and (17). Since a detailed knowledge of Mn-Mn and Mn-V exchanges is required in order to compute the ferromagnetically ordered S_z component, we set $S_z = 1/\sqrt{3}$ to simplify the calculation. As Fig. 6 shows, below a critical $J_\tau^* \approx 0.18\lambda$, pseudospins τ are polarized along z direction, while the transverse spin components pointing along the diagonal directions form the orthogonal structure shown in Fig. 5(b). Above the critical J_τ^* , the transverse spins rotate uniformly (the rotation is described by angle ϕ) while maintaining the orthogonal structure. At the same time, pseudospins develop a finite antiferro-orbital order along τ_y which is characterized by angle ψ . The calculation shows that at $J_\tau \gtrsim 10\lambda$, the spin anisotropy is already dominated by Eq. (17) as the angle $\phi \approx 0$ and the in-plane spins essentially point along either x or y axis.

VI. CONCLUSIONS

To summarize, we have proposed and studied a spin-orbital model for vanadium spinel MnV_2O_4 taking into account a large trigonal distortion at the vanadium sites. Instead of conventional t_{2g} triplet, our starting point is the doubly degenerate e_g eigenstates of the trigonal crystal field. By introducing a pseudospin-1/2 for the low-energy doublet, we have shown that the effective orbital interaction resulting from both the superexchange and

cooperative Jahn-Teller effect is described by a quantum 120° Hamiltonian on pyrochlore lattice. From both analytical and numerical calculations, we have found six classical ground states with collinear pseudospins perpendicular to either one of the three unit vectors characterizing the anisotropic interactions. The classical ground state is further shown to be stable against quantum fluctuations.

The ground-state structure obtained from our model is consistent with main experimental observations and *ab initio* calculation of MnV_2O_4 , namely, an antiferro-orbital order with tetragonal $I4_1/a$ space group, a density-modulation along orbital chains, and an orthogonal magnetic structure. The orbital order corresponding to the semiclassical ground states consists of two inequivalent orbital chains running along $\langle 110 \rangle$ and $\langle 1\bar{1}0 \rangle$ directions, similar to the so-called A -type antiferro-orbital order. However, the staggering of trigonal axes along orbital chains gives rise to a periodic variation of the electron density function, which is absent in the A -type order. Moreover, since the trigonal distortion breaks the approximate rotational symmetry of t_{2g} orbitals, orthogonal magnetic structure is shown to be stabilized by the staggering of the single-ion spin anisotropies.

The overall orientation of the orthogonal structure actually depends on the relative strength of effective orbital exchange J_τ and spin-orbit coupling λ . The experimentally proposed orthogonal structure¹⁴ with transverse vanadium spins pointing along either x or y axes is stabilized when $J_\tau > \lambda$. Using the large- J approach which assumes a dominant λ over superexchange energy scale, we have recently shown that the same orthogonal spin structure is stabilized when the predominant lattice distortion is of F_{1g} symmetry. In fact, without any Jahn-Teller distortion, the large- J ground state has a collinear antiferromagnetic order similar to the one proposed in Ref. 17. Noting that J_τ also includes contributions from F_{1g} phonons, results from the two complementary approaches (large trigonal field vs large- J) are actually consistent: stabilization of the experimentally proposed orthogonal structure requires a dominant F_{1g} distortion as well as a smaller spin-orbit coupling. This conclusion is also supported by recent *ab initio* calculation which shows that inclusion of spin-orbit coupling does not significantly change the spin-orbital order (a finite LS coupling, however, is still required to provide the spin anisotropies). Detailed analysis of Jahn-Teller phonons from first-principles calculation might help clarify the role of F_{1g} phonons.

Acknowledgments

The authors acknowledge G. Jackeli, V. Garlea, I. Rousochatzakis, O. Tchernyshyov, and R. Valentí for useful discussions. G.W.C. is particularly grateful to O. Tchernyshyov for sharing his insights and opinions on developing theoretical models of vanadium spinels.

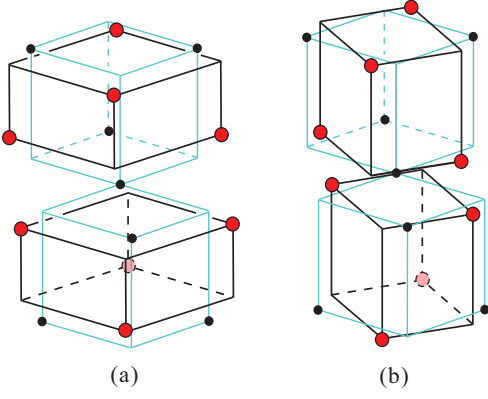


FIG. 7: $\mathbf{q} = 0$ lattice phonons with (a) E_g and (b) F_{1g} symmetries in a spinel structure. These normal modes are dominated by oxygen displacements. The red and black circles indicate oxygen and vanadium ions, respectively.

Appendix A: Phonon-mediated orbital exchange

In this Appendix, we derive the effective pseudospin interaction due to cooperative Jahn-Teller effect. The derivation presented here is based on a related work in Ref. 21. To explicitly take into account the cooperative nature of phonon-mediated orbital exchange, we consider coupling of orbitals to nonlocal lattice vibrations. In fact, a similar study based on local Einstein-like phonons gives an inconclusive result.²¹ To further simplify the discussion, we notice that all experimentally observed structural distortion in vanadium spinels preserves the lattice translational symmetry. We thus restrict our analysis to phonons with wavevector $\mathbf{q} = 0$.

Since orbitals mainly couple to oxygen ions, we focus on normal modes which are dominated by oxygen displacements. The 8 oxygen ions in a primitive unit cell of spinel form two tetrahedra related to each other by inversion symmetry. In the following, we confine ourselves to oxygen phonons with odd parity (coupling to even-parity oxygen modes cancels identically). Among the remaining modes, we find that the doublet E_g and triplet F_{1g} phonons are most effective in JT coupling. The E_g modes correspond to the tetragonal and orthorhombic distortions of the oxygen tetrahedra, whereas the triply degenerate F_{1g} modes represent rigid rotations of oxygen tetrahedra about the three cubic axes (Fig. 7).⁴⁰

As discussed in Sec. III, the orbital doublet (τ_x, τ_y) of trigonal crystal field couples to the E_g distortion of VO_6 octahedron [Eq. (9)]. To obtain the effective orbital interaction mediated by the above-mentioned lattice phonons, we first express the coordinates (δ_1, δ_2) describing the distortion of a local VO_6 octahedron in terms of coordinates of lattice E_g and F_{1g} phonons. The energy costs associated with the two modes are characterized by effective elastic constants k_{E_g} and $k_{F_{1g}}$, respectively. After inte-

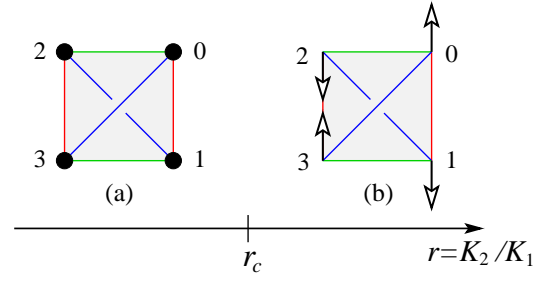


FIG. 8: Classical phase diagram of Hamiltonian Eq. (A1). The filled circle denotes $+\tau_z$ component of pseudospin. The ground-state orbital order depends on the ratio $r = K_2/K_1$. The boundary separating ferro-orbital from collinear antiferro-orbital states is given by $r_c = 8/3$.

grating out the phonons, we obtain

$$H_{\text{JT}} = -K_1 \sum_{\langle ij \rangle} \boldsymbol{\tau}_i \cdot \boldsymbol{\tau}_j + K_2 \sum_{\langle ij \rangle} (\boldsymbol{\tau}_i \cdot \hat{\mathbf{n}}_\alpha)(\boldsymbol{\tau}_j \cdot \hat{\mathbf{n}}_\alpha), \quad (\text{A1})$$

with the following effective exchange constants

$$K_1 = 2g^2/k_{E_g} + g^2/k_{F_{1g}}, \quad K_2 = 3g^2/k_{F_{1g}}. \quad (\text{A2})$$

The effective Hamiltonian (A1) contains two competing interactions: the K_1 term denotes an isotropic Heisenberg exchange, whereas the K_2 term represents the anisotropic 120° interaction introduced in Sec. II. A classical phase diagram of the above model is summarized in Fig. 8, where a ferro-orbital order is separated from the collinear antiferro-orbital ground state of the 120° model discussed previously. Note that the Heisenberg term has a ferromagnetic sign, hence favoring a ferro-orbital ordering. The ferro-orbital state is doubly degenerate with all pseudospins pointing along either $+\hat{\mathbf{z}}$ or $-\hat{\mathbf{z}}$ directions. On the other hand, pseudospins in the antiferro-orbital phase are in a collinear up-up-down-down configuration. As discussed in Sec. II, there are totally six degenerate antiferro-orbital states; the one shown in Fig. 8(b) is characterized by a nonzero order parameter $\mathbf{l}_{xy} = +\hat{\mathbf{y}}$. By comparing the energies, we find a phase boundary at $r_c = (K_2/K_1)_c = 8/3$.

Appendix B: Semiclassical approach to 120° model

Here we examine quantum corrections to the classical ground state of orbital 120° model on pyrochlore lattice. Our approach is based on a semiclassical Holstein-Primakoff expansion around the collinear state described by order parameter $\mathbf{l}_{xy} = +\hat{\mathbf{y}}$ [Fig. 3(c)]. To this end, we first generalize the 120° model to pseudospins \mathbf{T} of arbitrary length $|\mathbf{T}| = \sqrt{T(T+1)}$:

$$H_{120^\circ} = J_T \sum_{\langle ij \rangle} (\mathbf{T}_i \cdot \hat{\mathbf{n}}_\alpha)(\mathbf{T}_j \cdot \hat{\mathbf{n}}_\alpha), \quad (\text{B1})$$

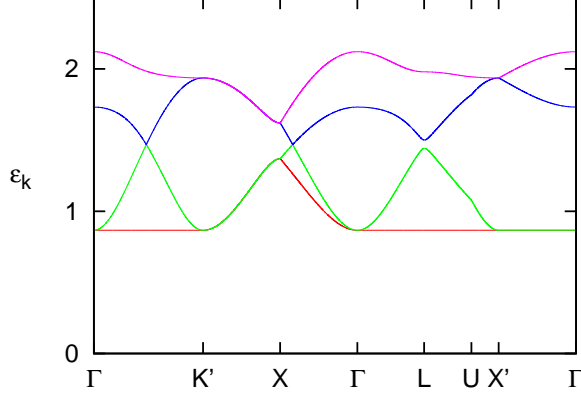


FIG. 9: Quasiparticle dispersions of the 120°-model. The energy $\varepsilon_{\mathbf{k}}$ is measured in unit of J_T . The various symmetry points in k -space are $\Gamma = (0, 0, 0)$, $K' = (1, 1, 0)$, $X = (1, 0, 0)$, $L = (\frac{1}{2}, \frac{1}{2}, \frac{1}{2})$, $U = (\frac{1}{4}, \frac{1}{4}, 1)$, and $X' = (0, 0, 1)$.

where J_T is an effective coupling constant. We then expand the Hamiltonian in powers of $1/T$ around the classical ground state using Holstein-Primakoff transformation. To simplify the calculation, we rotate the pseudospins around T_x axis such that

$$T_x = \tilde{T}_x, \quad T_y = \pm \tilde{T}_z, \quad T_z = \mp \tilde{T}_y, \quad (\text{B2})$$

where $+$ and $-$ signs refer to pseudospins along $[110]$ and $[1\bar{1}0]$ chains, respectively. The classical ground state in terms of rotated pseudospins is simply $\mathbf{T}_i = +T\hat{\mathbf{z}}$. We then apply the standard Holstein-Primakoff transformation:

$$\begin{aligned} \tilde{T}_z &= T - a^\dagger a, \\ \tilde{T}_+ &= \sqrt{2T - a^\dagger a} a \approx \sqrt{2T} a \\ \tilde{T}_- &= a^\dagger \sqrt{2T - a^\dagger a} \approx \sqrt{2T} a^\dagger, \end{aligned} \quad (\text{B3})$$

where a and a^\dagger satisfy the canonical boson commutation relations. Substituting Eq. (B3) into 120° Hamiltonian (6), we obtain $H_{120^\circ} = -6N_t J_T T^2 + H_2 + \dots$, where N_t is the number of unit cells, H_2 of order $\mathcal{O}(T)$ is the quadratic magnon Hamiltonian, and the omitted terms are of higher orders in $1/T$. We note that the linear term $H_1 \sim \mathcal{O}(T^{3/2})$ vanishes identically as expected for expansion around a classical ground state.

After Fourier transformation, the quadratic Hamiltonian reads

$$H_2 = \sum_{\mathbf{k}} \vec{a}_{\mathbf{k}}^\dagger \begin{pmatrix} \frac{3\tau}{2}\mathcal{I} + M_{\mathbf{k}} & M_{\mathbf{k}} \\ M_{\mathbf{k}} & \frac{3\tau}{2}\mathcal{I} + M_{\mathbf{k}} \end{pmatrix} \vec{a}_{\mathbf{k}}, \quad (\text{B4})$$

where $\vec{a}_{\mathbf{k}} = [a_0(\mathbf{k}), \dots, a_3(\mathbf{k}), a_0^\dagger(-\mathbf{k}), \dots, a_3^\dagger(-\mathbf{k})]^T$ is an 8-component column vector, \mathcal{I} is a 4×4 identity matrix, and

$$M_{\mathbf{k}} = \frac{T}{8} \begin{pmatrix} 0 & c_{yz} & c_{zx} & 4c_{xy} \\ c_{yz} & 0 & 4\bar{c}_{xy} & \bar{c}_{zx} \\ c_{zx} & 4\bar{c}_{xy} & 0 & \bar{c}_{yz} \\ 4c_{xy} & \bar{c}_{zx} & \bar{c}_{yz} & 0 \end{pmatrix}. \quad (\text{B5})$$

For convenience, we have defined $c_{\alpha\beta} = \cos[(k_\alpha + k_\beta)/4]$ and $\bar{c}_{\alpha\beta} = \cos[(k_\alpha - k_\beta)/4]$ (the lattice constant is set to 1). To diagonalize H_2 , we consider equation of motion for boson operator $\vec{a}_{\mathbf{k}}$:

$$i \frac{\partial \vec{a}_{\mathbf{k}}}{\partial t} = \begin{pmatrix} \frac{3\tau}{2}\mathcal{I} + M_{\mathbf{k}} & M_{\mathbf{k}} \\ -M_{\mathbf{k}} & -\frac{3\tau}{2}\mathcal{I} - M_{\mathbf{k}} \end{pmatrix} \vec{a}_{\mathbf{k}} \equiv \mathcal{L}_{\mathbf{k}} \vec{a}_{\mathbf{k}}. \quad (\text{B6})$$

From eigenvectors of matrix $\mathcal{L}_{\mathbf{k}}$, one can construct a canonical transformation $\vec{a}_{\mathbf{k}} = \mathcal{T}_{\mathbf{k}} \vec{c}_{\mathbf{k}}$, where matrix $\mathcal{T}_{\mathbf{k}}$ satisfies

$$\mathcal{T}_{\mathbf{k}}^\dagger \eta \mathcal{T}_{\mathbf{k}} = \eta, \quad \mathcal{T}_{\mathbf{k}}^{-1} \mathcal{L}_{\mathbf{k}} \mathcal{T}_{\mathbf{k}} = \eta \Lambda_{\mathbf{k}}. \quad (\text{B7})$$

Here the diagonal matrices $\eta = \text{diag}(\mathcal{I}, -\mathcal{I})$ and $\Lambda_{\mathbf{k}} = \text{diag}(\varepsilon_0(\mathbf{k}), \dots, \varepsilon_3(\mathbf{k}), \varepsilon_0(-\mathbf{k}), \dots, \varepsilon_3(-\mathbf{k}))$. Using Eq. (B7), the diagonalized Hamiltonian becomes

$$H_2 = \frac{1}{2} \sum_{\mathbf{k}} \vec{c}_{\mathbf{k}}^\dagger \Lambda_{\mathbf{k}} \vec{c}_{\mathbf{k}} = \sum_m \sum_{\mathbf{k}} \varepsilon_m(\mathbf{k}) c_m^\dagger(\mathbf{k}) c_m(\mathbf{k}). \quad (\text{B8})$$

By setting T to its physical value $1/2$, the numerically obtained dispersion $\varepsilon_m(\mathbf{k})$ along various symmetry directions of the Brillouin zone is shown in Fig. 9. The spectrum is fully gapped with an energy gap of order J_T , implying a small quantum correction. To confirm this, we also compute the harmonic correction to the sublattice ‘magnetization’ $\langle \tilde{T}_z \rangle = 1/2 - \langle a_i^\dagger a_i \rangle$. Using the explicit expression of the canonical transformation $\mathcal{T}_{\mathbf{k}}$:

$$a_s(\mathbf{k}) = u_{s,m}(\mathbf{k}) c_m(\mathbf{k}) + v_{s,m}(\mathbf{k}) c_m^\dagger(-\mathbf{k}), \quad (\text{B9})$$

the average quasiparticle number can be computed: $\langle a_i^\dagger a_i \rangle = (1/N_t) \sum_{\mathbf{k}} \langle a_s^\dagger(\mathbf{k}) a_s(\mathbf{k}) \rangle = \sum_m \sum_{\mathbf{k}} v_{s,m}^2$. The numerically obtained sublattice ‘magnetization’ is given by $\langle \tilde{T}_z \rangle \approx 1/2 - 0.02154$. The collinear ground states shown in Fig. 3 thus are stable against quantum fluctuations, at least at the harmonic order.

¹ H. F. Pen, J. van den Brink, D. I. Khomskii, and G. A. Sawatzky, Phys. Rev. Lett. **78**, 1323 (1997).

² P.G. Radaelli, Y. Horibe, M. J. Gutmann, H. Ishibashi,

C. H. Chen, R. M. Ibberson, Y. Koyama, Y.S. Hor, V. Kiryukhin, and S. W. Cheong, Nature (London) **416**, 155 (2002).

- ³ M. Schmidt, W. Ratcliff, II, P. G. Radaelli, K. Refson, N. M. Harrison, and S. W. Cheong, Phys. Rev. Lett. **92**, 056402 (2004).
- ⁴ Y. Horibe, M. Shingu, K. Kurushima, H. Ishibashi, N. Ikeda, K. Kato, Y. Motome, N. Furukawa, S. Mori, and T. Katsufuji, Phys. Rev. Lett. **96**, 086406 (2006).
- ⁵ S. Di Matteo, G. Jackeli, C. Lacroix, and N. B. Perkins, Phys. Rev. Lett. **93**, 077208 (2004).
- ⁶ D. I. Khomskii and T. Mizokawa, Phys. Rev. Lett. **94**, 156402 (2005).
- ⁷ R. Moessner and J. T. Chalker, Phys. Rev. Lett. **80**, 2929 (1998).
- ⁸ H. Mamiya, M. Onoda, T. Furubayashi, J. Tang, and I. Nakatani, J. Appl. Phys. **81**, 5289 (1997).
- ⁹ M. Reehuis, A. Krimmel, N. Büttgen, A. Loidl, A. Prokofiev, Eur. Phys. J. B **35**, 311 (2003).
- ¹⁰ M. Onoda and J. Hasegawa, J. Phys.: Condens. Matter **15**, 95 (2003).
- ¹¹ S.-H. Lee, D. Louca, H. Ueda, S. Park, T. J. Sato, M. Isobe, Y. Ueda, S. Rosenkranz, P. Zschack, J. Iniguez, Y. Qiu, R. Osborn, Phys. Rev. Lett. **93**, 15640 (2004).
- ¹² K. Adachi, T. Suzuki, K. Kato, K. Osaka, M. Takata, and T. Katsufuji, Phys. Rev. Lett. **95**, 197202 (2005).
- ¹³ T. Suzuki, M. Katsumura, K. Taniguchi, T. Arima, and T. Katsufuji, Phys. Rev. Lett. **98**, 127203 (2007).
- ¹⁴ V. O. Garlea, R. Jin, D. Mandrus, B. Roessli, Q. Huang, M. Miller, A. J. Schultz, and S. E. Nagler, Phys. Rev. Lett. **100**, 066404 (2008).
- ¹⁵ J.-H. Chung, J.-H. Kim, S.-H. Lee, T. J. Sato, T. Suzuki, M. Katsumura, and T. Katsufuji, Phys. Rev. B **77**, 054412 (2008).
- ¹⁶ H. Tsunetsugu and Y. Motome, Phys. Rev. B **68**, 060405(R) (2003).
- ¹⁷ O. Tchernyshyov, Phys. Rev. Lett. **93**, 157206 (2004).
- ¹⁸ S. Di Matteo, G. Jackeli, and N. B. Perkins, Phys. Rev. B **72**, 020408(R) (2005).
- ¹⁹ T. Maitra and R. Valentí, Phys. Rev. Lett. **99**, 126401 (2007).
- ²⁰ V. Pardo, S. Blanco-Canosa, F. Rivadulla, D.I. Khomskii, D. Baldomir, Hua Wu, and J. Rivas, Phys. Rev. Lett. **101**, 256403 (2008).
- ²¹ G.-W. Chern, PhD thesis, Johns Hopkins University, Baltimore (2008).
- ²² G.-W. Chern and N. B. Perkins, Phys. Rev. B **80**, 180409(R) (2009).
- ²³ S. Sarkar, T. Maitra, R. Valentí, and T. Saha-Dasgupta, Phys. Rev. Lett. **102**, 216405 (2009).
- ²⁴ S.-H. Baek, N. J. Curro, K.-Y. Choi, A. P. Reyes, P. L. Kuhns, H. D. Zhou, and C. R. Wiebe, Phys. Rev. **80**, 140406 (2009).
- ²⁵ Z. Nussinov, M. Biskup, L. Chayes, and J. v. d. Brink, Europhys. Lett. **67**, 990 (2004).
- ²⁶ M. Biskup, L. Chayes, and Z. Nussinov, Commun. Math. Phys. **255** 253 (2005).
- ²⁷ C. Castellani, C. R. Natoli, and J. Ranninger, Phys. Rev. B **18**, 4945 (1978); **18**, 4967 (1978); **18**, 5001 (1978).
- ²⁸ F. Mila, R. Shiina, F.-C. Zhang, A. Joshi, M. Ma, V. Anisimov, and T. M. Rice, Phys. Rev. Lett. **85**, 1714 (2000).
- ²⁹ S. Di Matteo, N.B. Perkins and C.R. Natoli, Phys. Rev. B **65**, 054413 (2002); N.B. Perkins, S. Di Matteo and C.R. Natoli, Phys. Rev. B **80**, 165106 (2009).
- ³⁰ V. I. Anisimov, M. A. Korotin, M. Zolff, T. Pruschke, K. Le Hur, and T. M. Rice, Phys. Rev. Lett. **83**, 364 (1999).
- ³¹ J. van den Brink, P. Horsch, F. Mack, and A. M. Oles, Phys. Rev. B **59**, 6795 (1999).
- ³² D. I. Khomskii and M. V. Mostovoy, J. Phys. A - Math. Gen. **36** 9197 (2003).
- ³³ The e_g system discussed in Refs. 31,32 refers to the degenerate orbitals $d_{3z^2-r^2}$ and $d_{x^2-y^2}$ in ions with, e.g. d^9 configuration. It should not be confused with the e_g doublet (2) derived from the t_{2g} orbitals.
- ³⁴ E. Zhao and W. V. Liu, Phys. Rev. Lett. **100**, 160403 (2008).
- ³⁵ C. Wu, Phys. Rev. Lett. **100**, 200406 (2008).
- ³⁶ K. I. Kugel and D. I. Khomskii, Sov. Phys. Usp. **25**, 231 (1982).
- ³⁷ Z. Nussinov and E. Fradkin, Phys. Rev. B, **71**, 195120 (2005); C. D. Batista and Z. Nussinov, Phys. Rev. B **72**, 045137 (2005).
- ³⁸ It should be noted that, contrary to the case of bipartite cubic lattice, antiferromagnetic and ferromagnetic 120° -models on pyrochlore lattice are inequivalent.
- ³⁹ G.-W. Chern, C. Fennie, and O. Tchernyshyov, Phys. Rev. B **74**, 060405(R) (2006).
- ⁴⁰ J. Himmrich and H. D. Lutz, Solid State Comm. **79**, 447 (1991).